Supplementary Information (SI) for EES Batteries.

Supplementary Information: Integrated Machine Learning-Molecular Dynamics Framework for Electrolyte Property Prediction

Srikant Sagireddy*[1,2,3], Nikhil Rampal*[1,2], Stephen E. Weitzner[1,2], and Liwen F. Wan*[1,2]

[1]Materials Science Division, Lawrence Livermore National Laboratory, Livermore, California, 94550, United States
[2]Laboratory for Energy Applications for the Future (LEAF), Lawrence Livermore National Laboratory, Livermore, California, 94550, United States
[3]Department of Chemical Engineering, Stanford University, Stanford, California, 94305, United States

*srikant@stanford.edu, rampal1@llnl.gov, wan6@llnl.gov

1 Generation of thermalized structures using Classical Molecular Dynamics Simulations

Classical molecular dynamics (CMD) simulations were performed using the LAMMPS software package [1]. Initial configurations for each electrolyte concentration were generated by randomly placing ions and solvent molecules in a periodic simulation cell using Packmol [2]. Interatomic interactions were described using the all-atom optimized potentials for liquid simulations (OPLS-AA) force field [3–5]. To implicitly account for electronic polarization effects in condensed-phase electrolytes, ionic partial charges were uniformly scaled to 80% of their nominal values [5]. Long-range electrostatic interactions were computed using the particle-particle particle–mesh (PPPM) method [6] with a relative force accuracy of 1×10^{-4}. Nosé-Hoover thermostat and barostat [7, 8] were employed to maintain constant temperature and pressure. Each system was equilibrated for 10 ns in the isothermal–isobaric (NPT) ensemble at 298 K and 1 bar to achieve stable liquid densities [9, 10], with a timestep of 1 fs.

Following equilibration, representative solvation structures were extracted from the CMD trajectories using an in-house Python analysis workflow based on well-defined geometric cutoff radii, derived from Li-molecule radial distribution function (RDFs) of each electrolyte system, and were subsequently used for downstream DFT and ML analyses. The first solvation shell cutoff was defined as the position of the first minimum in the Li–molecule RDF (ranging between 3 and 4$\mathring{A}$); a molecule was included in the first solvation shell if it fell within this cutoff, with periodic boundary conditions applied throughout. To construct secondary solvation shell structures, the second minimum of the Li–molecule RDF was used as the cutoff to capture molecules in the second coordination sphere; a further variant additionally included anion species within the secondary shell, corresponding to the S+A configurations analyzed in Fig. 3F and G. Solvation environments were classified by the molecular composition of the extracted first shell: clusters containing no anion molecules were designated as solvent-separated ion pairs (SSIPs), while those containing one or more anion molecules were referred as contact ion pairs (CIPs). Coordination number was defined as the total number of molecules, solvent or anion, present in the first solvation shell. Structures were sampled at regular intervals of 100 MD frames to ensure statistical independence of the extracted configurations.

2 Dataset Splitting and Test Set Composition

The filtered OMol25 battery electrolyte dataset comprises 24,228 structures representing lithium-containing electrolyte systems with coordination numbers between 3 and 10, excluding aqueous samples. We partitioned this dataset using random splitting with an 80/10/10 ratio for training, validation, and test sets. The validation set was used exclusively for monitoring training progress, while the test set remained completely held out during all stages of model development. Model performance metrics reported in the text were computed on this held-out test set.

3 DFT Calculations Details

All density functional theory (DFT) calculations were performed using ORCA 6.0.0 [11, 12] with the ωB97M-V range-separated hybrid meta-GGA functional and the def2-TZVPD basis set [13–15]. We employed the RI-J [16] and COSX [17] integral acceleration techniques, DEFGRID3 grid settings, and tight SCF convergence criteria. Frontier orbital energies (HOMO and LUMO levels) were calculated using the delta-SCF (Δ-SCF) method to provide more reliable energy level predictions compared to Kohn-Sham eigenvalues.

In the Δ-SCF method, the electron affinities (EA) and ionization energies (IE) are calculated by taking the difference between the calculated energy of a species and the calculated energy of that species with one additional or one less electron. The negative EA corresponds to the energy of the LUMO level, while the negative IE corresponds to the energy of the HOMO level [18].

4 Results from training larger parameter model

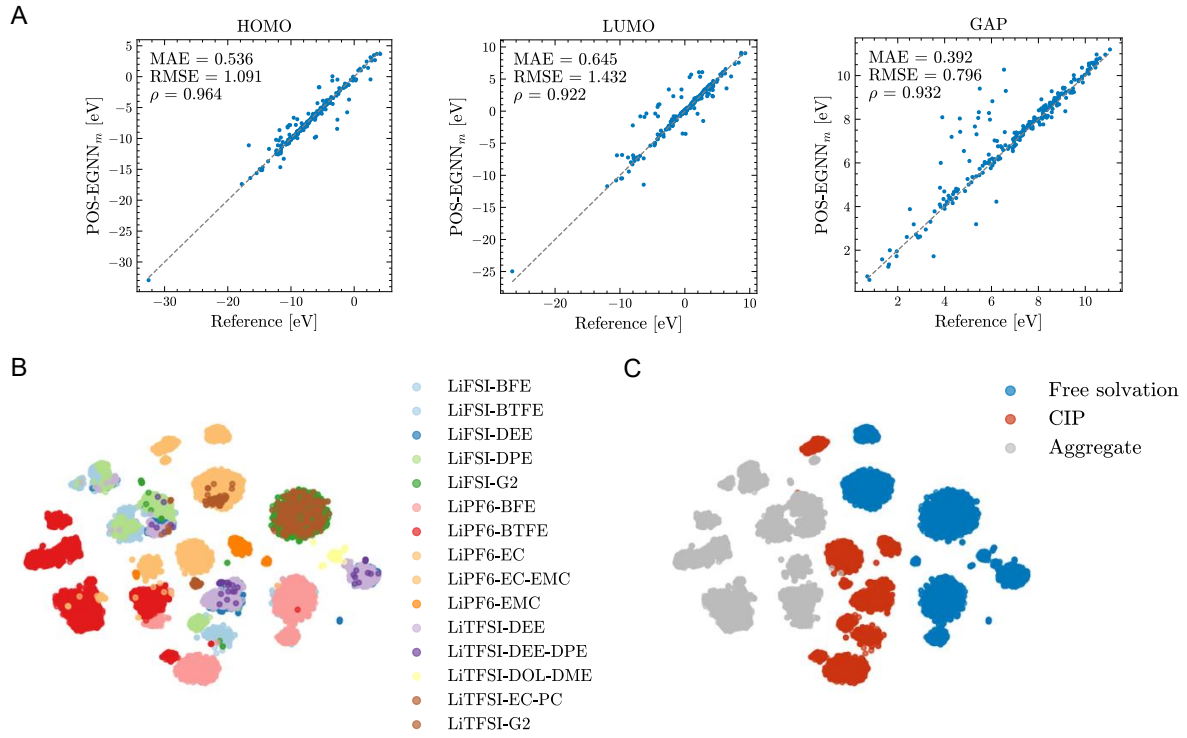

Figure S1. Medium-sized model results. (A) Parity plots comparing the predicted HOMO energy (HOMO), LUMO energy (LUMO), and HOMO-LUMO gap (GAP) across the OMol25 lithium battery electrolyte test set for the medium-sized model. (B, C) t-SNE projection of Li-ion node embeddings colored by solvent and anion composition (B) or solvation shell speciation (C).

Table S1. Medium model predictions compared to DFT calculations across different electrolyte systems and local speciation. Error is calculated as DFT - ML.

Electrolyte	Speciation	HOMO [eV]			LUMO [eV]		
		Medium	DFT	Error	Medium	DFT	Error
LiFSI-G2	SSIP	-12.3	-12.7	-0.4	-1.23	-1.70	-0.47
	CIP	-9.99	-9.31	0.68	-0.21	0.26	0.47
LiTFSI-G2	SSIP	-12.9	-12.8	0.1	-1.78	-1.64	0.14
LiPF6-EC	SSIP	-13.6	-13.2	0.4	-2.13	-1.56	0.57
	CIP	-10.8	-10.8	0.0	-0.08	0.11	0.19
LiPF6-EMC	SSIP	-13.7	-13.3	0.4	-2.12	-1.75	0.37
	CIP	-12.3	-11.2	1.1	-2.15	0.19	2.34
LiPF6-EC-EMC	SSIP	-3.98	-6.89	-2.91	-0.26	-5.49	-5.23
	CIP	-4.19	-4.52	-0.33	0.80	-1.96	-2.76
LiTFSI-EC-PC	SSIP	-13.1	-12.9	0.2	-1.38	-1.38	0.0
	CIP	-10.3	-9.79	0.51	-0.02	0.20	0.22
LiFSI-DEE	SSIP	-13.8	-13.5	0.3	-2.09	-1.83	0.26
	CIP	-9.19	-8.97	0.22	-0.23	-0.09	0.14
LiTFSI-DEE	SSIP	-13.8	-13.5	0.3	-2.08	-1.82	0.26
	CIP	-10.9	-10.6	0.3	0.03	0.26	0.23
LiFSI-DPE	CIP	-10.2	-10.0	0.2	0.30	0.44	0.14
LiTFSI-DEE-DPE	SSIP	-13.3	-13.0	0.3	-1.89	-1.80	0.09
	CIP	-9.58	-8.86	0.72	-0.05	0.10	0.15
LiTFSI-DOL-DME	SSIP	-10.4	-11.1	-0.7	-1.78	-4.08	-2.3
LiFSI-BFE	SSIP	-14.5	-14.2	0.3	-2.15	-1.87	0.28
	CIP	-9.02	-8.81	0.21	-0.27	-0.14	0.13
LiPF6-BFE	SSIP	-14.3	-14.0	0.3	-2.08	-1.82	0.26
	CIP	-11.0	-11.0	0.0	0.22	0.22	0.0
LiFSI-BTFE	CIP	-10.1	-10.1	0.0	0.16	0.17	0.01
LiPF6-BTFE	SSIP	-14.2	-14.1	0.1	-1.97	-1.88	0.09
	CIP	-11.9	-12.3	-0.4	-0.26	-0.10	0.16

5 Stratified error analysis

To quantify how model performance varies with solvent composition complexity, we categorize the electrolyte systems in Table 2 into three groups: (1) single-component solvents, (2) structurally similar solvent mixtures, and (3) structurally dissimilar solvent mixtures, and report the mean absolute error (MAE) for HOMO and LUMO predictions within each category.

Table S2. Prediction errors broken down by solvent combination type. MAE values are computed from Table 2 of the main text across SSIP and CIP configurations.

Category	Systems	MAE [eV]	
		HOMO	LUMO
Single-component	LiFSI-G2, LiTFSI-G2, $LiPF_6$-EC, $LiPF_6$-EMC, LiFSI-DEE, LiTFSI-DEE, LiFSI-DPE, LiFSI-BFE, $LiPF_6$-BFE, LiFSI-BTFE, $LiPF_6$-BTFE	0.24	0.29
Structurally similar mixtures	LiTFSI-EC-PC, LiTFSI-DEE-DPE	0.38	0.15
Structurally dissimilar mixtures	$LiPF_6$-EC-EMC, LiTFSI-DOL-DME	3.54	1.76

Single-component systems achieve sub-0.29 eV MAE for both HOMO and LUMO, and structurally similar mixtures (EC/PC, both cyclic carbonates; DEE/DPE, both linear ethers) perform comparably, with HOMO MAE below 0.38 eV. The breakdown occurs specifically for structurally dissimilar mixtures:

$LiPF_6$-EC-EMC (cyclic carbonate plus linear ester) and LiTFSI-DOL-DME (cyclic ether plus linear ether) show HOMO MAEs exceeding 3.5 eV. In these systems, structurally distinct solvents compete for Li coordination, generating mixed first-shell geometries. The cooperative effect is that neither solvent's individual coordination geometry accurately describes the mixed environment, and the model cannot reliably interpolate between the single-component structures.

6 Electrochemical stability windows

Table S3. Electrochemical stability windows for different electrolyte systems.

Electrolyte	Cathodic Limit [V]	Anodic Limit [V]	Window Width [V]
LiFSI-G2	1.75 ± 0.07	8.81 ± 0.86	7.06
LiTFSI-G2	1.74 ± 0.06	12.85 ± 0.13	11.11
LiPF6-EC	1.97 ± 0.20	10.68 ± 0.42	8.71
LiPF6-EMC	2.00 ± 0.20	11.29 ± 0.31	9.29
LiPF6-EC-EMC	5.05 ± 1.16	10.15 ± 1.01	5.10
LiTFSI-EC-PC	1.58 ± 0.16	9.06 ± 0.46	7.48
LiFSI-DEE	2.39 ± 0.81	9.68 ± 0.33	7.29
LiTFSI-DEE	2.16 ± 0.10	9.85 ± 0.31	7.69
LiFSI-DPE	-0.45 ± 0.14	10.08 ± 0.23	10.54
LiTFSI-DEE-DPE	2.11 ± 0.14	9.85 ± 0.25	7.74
LiTFSI-DOL-DME	1.68 ± 0.19	12.39 ± 1.55	10.71
LiFSI-BFE	1.83 ± 0.12	9.53 ± 0.36	7.70
LiPF6-BFE	1.83 ± 0.14	11.04 ± 0.30	9.21
LiFSI-BTFE	-0.28 ± 0.24	9.88 ± 0.33	10.15
LiPF6-BTFE	1.63	11.49 ± 0.39	9.86

7 Literature DFT benchmarks for electrolyte

Table S4. Literature comparison of HOMO and LUMO energy levels for different solvation structures.

Electrolyte	Speciation	HOMO [eV]	LUMO [eV]	Level of Theory	Reference
LiFSI	Ion	-8.81	-1.41	B3LYP/6–311++G(d,p)	[19]
LiFSI-DEE	SSIP	-7.77	-0.61	B3LYP/6–311++G(d,p)	[20]
	CIP	-7.02	-0.73	B3LYP/6–311++G(d,p)	[20]
LiTFSI-G2	SSIP	-6.21	-0.89	PBE/6–31+G(d,p)	[21]

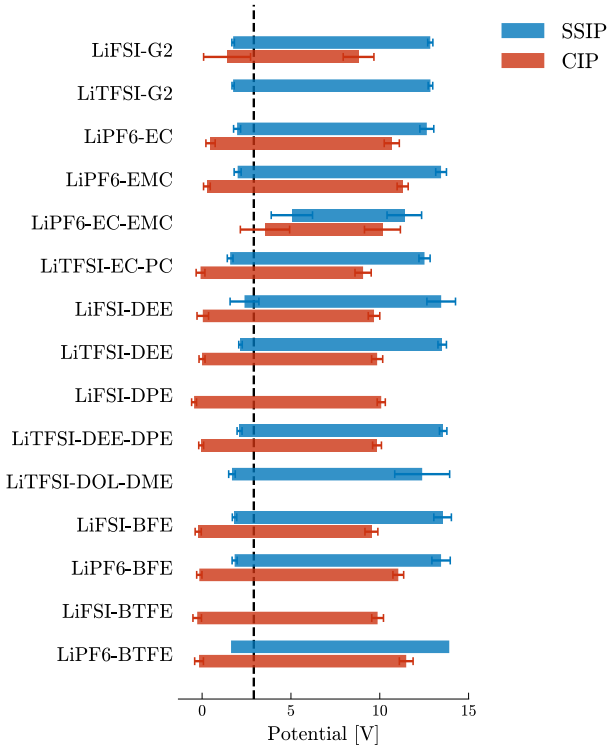

Figure S2. Electrochemical windows of Li-ion battery electrolytes. Blue bars indicate the potential range for which the freely solvated structures are stable. Red bars indicate the potential range for which the CIP structures are stable. The lithium metal Fermi level is indicated with a dashed black line. The error bars represent the first standard deviation in predicted values, representing the spread in sampled solvation structures from MD simulations.

8 Solvation size effects

Table S5. HOMO and LUMO values (eV) for different electrolyte systems across solvation shell configurations where primary solvation shell is SSIP. P: Primary shell, S: Secondary shell, S+A: Secondary shell with anion.

Electrolyte	**HOMO [eV]**			**LUMO [eV]**		
	P	S	S+A	P	S	S+A
LiFSI-BFE	-13.31 ± 0.27	-11.11 ± 0.20	-8.49 ± 0.44	-1.78 ± 0.10	-1.19 ± 0.11	0.38 ± 0.17
LiFSI-DEE	-13.61 ± 0.13	-11.47 ± 0.06	-8.82 ± 0.31	-2.18 ± 0.06	-1.53 ± 0.07	0.01 ± 0.15
LiPF6-BFE	-13.27 ± 0.32	-11.10 ± 0.28	-9.03 ± 0.38	-1.79 ± 0.11	-1.23 ± 0.14	0.29 ± 0.16
LiPF6-EC	-13.62 ± 0.23	-11.30 ± 0.59	-9.74 ± 0.35	-2.24 ± 0.18	-2.01 ± 0.23	-0.66 ± 0.30
LiPF6-EMC	-13.70 ± 0.17	-11.89 ± 0.00	-10.21 ± 0.19	-2.17 ± 0.14	-1.39 ± 0.00	0.08 ± 0.09
LiTFSI-DEE	-13.58 ± 0.14	-11.36 ± 0.16	-8.76 ± 0.38	-2.19 ± 0.06	-1.46 ± 0.06	-0.12 ± 0.13

Table S6. HOMO and LUMO values (eV) for different electrolyte systems across solvation shell configurations where primary solvation shell is CIP. P: Primary shell, S: Secondary shell, S+A: Secondary shell with anion.

Electrolyte	**HOMO [eV]**			**LUMO [eV]**		
	P	S	S+A	P	S	S+A
LiFSI-BFE	-9.54 ± 0.35	-8.98 ± 0.34	-6.80 ± 0.47	0.22 ± 0.17	0.52 ± 0.17	1.98 ± 0.21
LiFSI-DEE	-9.69 ± 0.30	-9.16 ± 0.14	-7.04 ± 0.45	0.01 ± 0.18	0.30 ± 0.09	1.75 ± 0.15
LiPF6-BFE	-11.10 ± 0.22	-9.03 ± 0.30	-7.19 ± 0.42	0.15 ± 0.15	0.41 ± 0.17	2.01 ± 0.21
LiPF6-EC	-11.38 ± 0.32	-10.08 ± 0.25	-7.93 ± 0.48	-0.56 ± 0.30	-0.32 ± 0.22	1.04 ± 0.32
LiPF6-EMC	-11.60 ± 0.19	-9.97 ± 0.30	-8.18 ± 0.44	-0.32 ± 0.21	0.34 ± 0.08	1.85 ± 0.11
LiTFSI-DEE	-9.91 ± 0.31	-9.23 ± 0.24	-7.04 ± 0.38	0.03 ± 0.18	0.29 ± 0.13	1.69 ± 0.20

9 Partial desolvation effect

Table S7. HOMO values (eV) for SSIP systems as a function of number of solvent molecules.

Electrolyte	**1 Solv.**	**2 Solv.**	**3 Solv.**	**4 Solv.**
LiFSI-BFE	–	-14.32 ± 0.15	-13.31 ± 0.27	–
LiFSI-DEE	-12.06 ± 2.52	-13.57 ± 0.70	-13.61 ± 0.25	-13.61 ± 0.13
LiFSI-G2	–	-12.84 ± 0.15	–	–
LiPF6-BFE	–	-14.33 ± 0.15	-13.27 ± 0.32	-12.43 ± 0.24
LiPF6-BTFE	–	–	-13.91 ± 0.00	–
LiPF6-EC	–	–	–	-13.62 ± 0.24
LiPF6-EMC	–	–	–	-13.70 ± 0.17
LiTFSI-DEE	–	–	–	-13.58 ± 0.14
LiTFSI-G2	–	-12.85 ± 0.13	–	–

Table S8. LUMO values (eV) for SSIP systems as a function of number of solvent molecules.

Electrolyte	**1 Solv.**	**2 Solv.**	**3 Solv.**	**4 Solv.**
LiFSI-BFE	–	-1.97 ± 0.07	-1.78 ± 0.10	–
LiFSI-DEE	-3.86 ± 1.90	-4.71 ± 0.42	-4.05 ± 0.88	-2.18 ± 0.06
LiFSI-G2	–	-1.75 ± 0.07	–	–
LiPF6-BFE	–	-2.00 ± 0.12	-1.79 ± 0.11	-1.63 ± 0.12
LiPF6-BTFE	–	–	-1.63 ± 0.00	–
LiPF6-EC	–	–	–	-2.24 ± 0.18
LiPF6-EMC	–	–	–	-2.17 ± 0.14
LiTFSI-DEE	–	–	–	-2.19 ± 0.06
LiTFSI-G2	–	-1.74 ± 0.06	–	–

Table S9. GAP values (eV) for SSIP systems as a function of number of solvent molecules.

Electrolyte	**1 Solv.**	**2 Solv.**	**3 Solv.**	**4 Solv.**
LiFSI-BFE	–	12.35 ± 0.13	11.52 ± 0.30	–
LiFSI-DEE	8.20 ± 0.85	8.85 ± 0.98	9.55 ± 1.10	11.43 ± 0.14
LiFSI-G2	–	11.10 ± 0.16	–	–
LiPF6-BFE	–	12.33 ± 0.17	11.47 ± 0.33	10.80 ± 0.26
LiPF6-BTFE	–	–	12.28 ± 0.00	–
LiPF6-EC	–	–	–	11.38 ± 0.32
LiPF6-EMC	–	–	–	11.53 ± 0.17
LiTFSI-DEE	–	–	–	11.39 ± 0.15
LiTFSI-G2	–	11.11 ± 0.14	–	–

Table S10. HOMO values (eV) for CIP systems as a function of number of solvent molecules.

Electrolyte	**1 Solv.**	**2 Solv.**	**3 Solv.**	**4 Solv.**
LiFSI-BFE	–	-9.54 ± 0.35	-9.30 ± 0.45	–
LiFSI-BTFE	–	-9.87 ± 0.33	-10.14 ± 0.00	–
LiFSI-DEE	-9.75 ± 0.00	-9.61 ± 0.00	-9.69 ± 0.30	-9.51 ± 0.24
LiFSI-DPE	–	-10.10 ± 0.21	-9.45 ± 0.21	–
LiFSI-G2	–	-8.81 ± 0.86	–	–
LiPF6-BFE	–	-11.10 ± 0.22	-10.31 ± 0.35	–
LiPF6-BTFE	-12.06 ± 0.24	-11.56 ± 0.30	-11.01 ± 0.25	-10.46 ± 0.00
LiPF6-EC	–	–	-11.38 ± 0.32	-10.78 ± 0.27
LiPF6-EMC	–	–	-11.60 ± 0.19	-11.11 ± 0.20
LiTFSI-DEE	–	-10.82 ± 0.00	-9.91 ± 0.31	-9.68 ± 0.24

Table S11. LUMO values (eV) for CIP systems as a function of number of solvent molecules.

Electrolyte	**1 Solv.**	**2 Solv.**	**3 Solv.**	**4 Solv.**
LiFSI-BFE	–	0.22 ± 0.17	0.24 ± 0.19	–
LiFSI-BTFE	–	0.27 ± 0.24	0.55 ± 0.00	–
LiFSI-DEE	-2.04 ± 0.00	-1.25 ± 0.00	0.01 ± 0.18	-0.02 ± 0.13
LiFSI-DPE	–	0.45 ± 0.14	0.32 ± 0.15	–
LiFSI-G2	–	-1.41 ± 1.32	–	–
LiPF6-BFE	–	0.15 ± 0.15	0.27 ± 0.14	–
LiPF6-BTFE	-0.35 ± 0.29	0.16 ± 0.19	0.41 ± 0.16	0.54 ± 0.00
LiPF6-EC	–	–	-0.56 ± 0.30	-0.48 ± 0.25
LiPF6-EMC	–	–	-0.32 ± 0.21	-0.24 ± 0.17
LiTFSI-DEE	–	0.13 ± 0.00	0.03 ± 0.18	-0.06 ± 0.12

Table S12. GAP values (eV) for CIP systems as a function of number of solvent molecules.

Electrolyte	1 Solv.	2 Solv.	3 Solv.	4 Solv.
LiFSI-BFE	–	9.76 ± 0.46	9.54 ± 0.59	–
LiFSI-BTFE	–	10.14 ± 0.46	10.70 ± 0.00	–
LiFSI-DEE	7.71 ± 0.00	8.36 ± 0.00	9.70 ± 0.42	9.49 ± 0.30
LiFSI-DPE	–	10.55 ± 0.28	9.77 ± 0.25	–
LiFSI-G2	–	7.40 ± 2.17	–	–
LiPF6-BFE	–	11.25 ± 0.24	10.57 ± 0.36	–
LiPF6-BTFE	11.71 ± 0.26	11.71 ± 0.39	11.42 ± 0.32	11.00 ± 0.00
LiPF6-EC	–	–	10.82 ± 0.40	10.30 ± 0.37
LiPF6-EMC	–	–	11.28 ± 0.20	10.87 ± 0.22
LiTFSI-DEE	–	10.95 ± 0.00	9.94 ± 0.43	9.62 ± 0.30

10 SMI-TED model

SMI-TED (SMILES Transformer Encoder-Decoder) is an encoder-decoder foundation model for molecular property prediction developed by Soares et al. [22]. The model was pre-trained on a curated dataset of 91 million molecular sequences from PubChem. The base SMI-TED289M model contains 289 million parameters with a transformer-based architecture consisting of 12 layers, 12 attention heads, and a hidden dimension of 768. The model takes SMILES strings as input, which are tokenized into a vocabulary of 2,993 tokens with a maximum sequence length of 202 tokens. These tokens are processed through a bidirectional transformer encoder to generate contextualized embeddings. Unlike standard encoder-only models, SMI-TED includes a decoder component that reconstructs the input SMILES from a compressed latent representation.

For downstream tasks, the latent space representations are extracted and used as input to task-specific prediction heads. We fine-tuned the publicly released pre-trained model on the QM9 dataset [23] to predict the HOMO, LUMO, and HOMO-LUMO gap.

Table S13. HOMO values (eV) predicted by POS-EGNN and SMI-TED for various solvent systems.

Solvent	POS-EGNN	SMI-TED	Difference
G2	−12.64	−6.81	−5.83
EC	−11.26	−7.75	−3.51
EMC	−11.53	−7.33	−4.20
EC-EMC	−10.69	−7.48	−3.21
EC-PC	−11.07	−7.75	−3.32
DEE	−10.58	−6.75	−3.83
DPE	−7.21	−6.68	−0.52
DEE-DPE	−10.68	−6.74	−3.94
DOL-DME	−12.39	−6.89	−5.50
BFE	−11.80	−7.24	−4.56
BTFE	−5.79	−7.93	2.14

Table S14. LUMO values (eV) predicted by POS-EGNN and SMI-TED for various solvent systems.

Solvent	POS-EGNN	SMI-TED	Difference
G2	−1.67	2.18	−3.86
EC	−0.85	0.96	−1.81
EMC	−0.45	1.36	−1.81
EC-EMC	−4.17	1.24	−5.41
EC-PC	−0.84	1.00	−1.85
DEE	−0.33	2.50	−2.83
DPE	2.28	2.50	−0.22
DEE-DPE	−0.35	2.50	−2.85
DOL-DME	−1.68	2.33	−4.01
BFE	−0.58	2.13	−2.71
BTFE	4.26	1.85	2.41

Table S15. GAP values (eV) predicted by POS-EGNN and SMI-TED for various solvent systems.

Solvent	POS-EGNN	SMI-TED	Difference
G2	10.96	9.08	1.88
EC	10.41	9.03	1.38
EMC	11.09	9.01	2.08
EC-EMC	6.52	9.03	−2.51
EC-PC	10.23	9.03	1.19
DEE	10.25	9.37	0.88
DPE	9.49	9.26	0.23
DEE-DPE	10.33	9.27	1.06
DOL-DME	10.71	9.37	1.33
BFE	11.22	9.22	1.99
BTFE	10.05	9.85	0.20

References

1. Thompson, A. P. *et al.* LAMMPS-a flexible simulation tool for particle-based materials modeling at the atomic, meso, and continuum scales. *Computer Physics Communications* **271,** 108171 (2022).
2. Martínez, L., Andrade, R., Birgin, E. G. & Martínez, J. M. PACKMOL: A package for building initial configurations for molecular dynamics simulations. *Journal of computational chemistry* **30,** 2157–2164 (2009).
3. Jorgensen, W. L., Maxwell, D. S. & Tirado-Rives, J. Development and testing of the OPLS all-atom force field on conformational energetics and properties of organic liquids. *Journal of the American Chemical Society* **118,** 11225–11236 (1996).
4. Sambasivarao, S. V. & Acevedo, O. Development of OPLS-AA force field parameters for 68 unique ionic liquids. *Journal of chemical theory and computation* **5,** 1038–1050 (2009).
5. Doherty, B., Zhong, X., Gathiaka, S., Li, B. & Acevedo, O. Revisiting OPLS force field parameters for ionic liquid simulations. *Journal of chemical theory and computation* **13,** 6131–6145 (2017).
6. Hockney, R. W. & Eastwood, J. W. *Computer simulation using particles* (crc Press, 2021).
7. Nosé, S. A unified formulation of the constant temperature molecular dynamics methods. *The Journal of chemical physics* **81,** 511–519 (1984).
8. Hoover, W. G. Canonical dynamics: Equilibrium phase-space distributions. *Physical review A* **31,** 1695 (1985).
9. Shinoda, W., Shiga, M. & Mikami, M. Rapid estimation of elastic constants by molecular dynamics simulation under constant stress. *Physical Review B* **69,** 134103 (2004).

10. Martyna, G. J., Tobias, D. J. & Klein, M. L. Constant pressure molecular dynamics algorithms. *The Journal of chemical physics* **101,** 4177–4189 (1994).

11. Neese, F. Software update: The ORCA program system—Version 5.0. en. *WIREs Computational Molecular Science* **12,** e1606. ISSN: 1759-0884 (2022).

12. Neese, F. Software Update: The ORCA Program System—Version 6.0. en. *WIREs Computational Molecular Science* **15,** e70019. ISSN: 1759-0884 (2025).

13. Weigend, F. & Ahlrichs, R. Balanced basis sets of split valence, triple zeta valence and quadruple zeta valence quality for H to Rn: Design and assessment of accuracy. en. *Physical Chemistry Chemical Physics* **7.** Publisher: The Royal Society of Chemistry, 3297–3305. ISSN: 1463-9084 (Aug. 2005).

14. Rappoport, D. & Furche, F. Property-optimized Gaussian basis sets for molecular response calculations. *The Journal of Chemical Physics* **133,** 134105. ISSN: 0021-9606 (Oct. 2010).

15. Rappoport, D. Property-optimized Gaussian basis sets for lanthanides. *The Journal of Chemical Physics* **155,** 124102. ISSN: 0021-9606 (Sept. 2021).

16. Neese, F. An improvement of the resolution of the identity approximation for the formation of the Coulomb matrix. en. *Journal of Computational Chemistry* **24,** 1740–1747. ISSN: 0192-8651, 1096-987X (Nov. 2003).

17. Helmich-Paris, B., de Souza, B., Neese, F. & Izsák, R. An improved chain of spheres for exchange algorithm. *The Journal of Chemical Physics* **155,** 104109. ISSN: 0021-9606 (Sept. 2021).

18. Martin, R. M. *Electronic Structure: Basic Theory and Practical Methods* en. ISBN: 978-0-521-78285-2 (Cambridge University Press, Apr. 2004).

19. Ren, X. *et al.* A Biocompatible Deep Eutectic Electrolyte Enables Ultra-Fast Charging in Lithium-Ion Batteries. *Advanced Functional Materials,* 2500464 (2025).

20. Pham, T. D., Bin Faheem, A., Kim, J., Oh, H. M. & Lee, K.-K. Practical High-Voltage Lithium Metal Batteries Enabled by Tuning the Solvation Structure in Weakly Solvating Electrolyte. *Small* **18,** 2107492 (2022).

21. Carrillo-Bohórquez, O., Kuroda, D. G. & Kumar, R. Atomistic Insights into Lithium–Glyme Solvate Ionic Liquids: Effects of Chain Length and Anion Coordination. en. *The Journal of Physical Chemistry B* **129,** 10072–10083 (Oct. 2025).

22. Soares, E. *et al.* An open-source family of large encoder-decoder foundation models for chemistry. *Communications Chemistry* **8,** 193 (2025).

23. Ramakrishnan, R., Dral, P. O., Rupp, M. & Von Lilienfeld, O. A. Quantum chemistry structures and properties of 134 kilo molecules. en. *Scientific Data* **1,** 140022. ISSN: 2052-4463 (Aug. 2014).